

---

# Princeton Plasma Physics Laboratory

---

PPPL-

PPPL-



Prepared for the U.S. Department of Energy under Contract DE-AC02-09CH11466.

# Princeton Plasma Physics Laboratory

## Report Disclaimers

---

### Full Legal Disclaimer

This report was prepared as an account of work sponsored by an agency of the United States Government. Neither the United States Government nor any agency thereof, nor any of their employees, nor any of their contractors, subcontractors or their employees, makes any warranty, express or implied, or assumes any legal liability or responsibility for the accuracy, completeness, or any third party's use or the results of such use of any information, apparatus, product, or process disclosed, or represents that its use would not infringe privately owned rights. Reference herein to any specific commercial product, process, or service by trade name, trademark, manufacturer, or otherwise, does not necessarily constitute or imply its endorsement, recommendation, or favoring by the United States Government or any agency thereof or its contractors or subcontractors. The views and opinions of authors expressed herein do not necessarily state or reflect those of the United States Government or any agency thereof.

### Trademark Disclaimer

Reference herein to any specific commercial product, process, or service by trade name, trademark, manufacturer, or otherwise, does not necessarily constitute or imply its endorsement, recommendation, or favoring by the United States Government or any agency thereof or its contractors or subcontractors.

---

## PPPL Report Availability

### Princeton Plasma Physics Laboratory:

<http://www.pppl.gov/techreports.cfm>

### Office of Scientific and Technical Information (OSTI):

<http://www.osti.gov/bridge>

---

### Related Links:

[U.S. Department of Energy](#)

[Office of Scientific and Technical Information](#)

[Fusion Links](#)

# Benchmarking ICRF full-wave solvers for ITER

v8 Dec 31, 2010

R. V. Budny<sup>1</sup>, L. Berry<sup>2</sup>, R. Bilato<sup>3</sup>, P. Bonoli<sup>4</sup>, M. Brambilla<sup>3</sup>, R. J. Dumont<sup>5</sup>, A. Fukuyama<sup>6</sup>, R. Harvey<sup>7</sup>, E. F. Jaeger<sup>8</sup>, K. Indireskumar<sup>1</sup>, E. Lerche<sup>9</sup>, D. McCune<sup>1</sup>, C. K. Phillips<sup>1</sup>, V. Vdovin<sup>10</sup>, J. Wright<sup>4</sup>, and members of the ITPA-IOS

<sup>1</sup>PPPL, P.O. Box 451, Princeton, NJ 08543, USA, <sup>2</sup>ORNL, PO Box 2008, Oak Ridge, TN 37831, USA, <sup>3</sup>Max-Planck-Institut für Plasmaphysik, Garching, Germany, <sup>4</sup>MIT Plasma Science and Fusion Center, 77 Mass. Avenue, Cambridge, MA 02139, USA, <sup>5</sup>CEA, IRFM, F-13108 Saint-Paul-lez-Durance, France, <sup>6</sup>Department of Nuclear Engineering, Kyoto University, Kyoto, 606-8501, Japan, <sup>7</sup>CompX, Box 2672, Del Mar, CA 92014, USA, <sup>8</sup>XCEL Engineering Inc., 1066 Commerce Park Dr., Oak Ridge, TN 37830, USA, <sup>9</sup>LPP-ERM/KMS, Association Euratom-Belgian State, TEC Partner, Brussels, Belgium, <sup>10</sup>RRC Kurchatov Institute Tokamaks Physics Institute, Russia

e-mail contact of main author: budny@princeton.edu

**Abstract** Benchmarking of full-wave solvers for ICRF simulations is performed using plasma profiles and equilibria obtained from integrated self-consistent modeling predictions of four ITER plasmas. One is for a high performance baseline (5.3 T, 15 MA) DT H-mode. The others are for half-field, half-current plasmas of interest for the pre-activation phase with bulk plasma ion species being either hydrogen or He<sup>4</sup>. The predicted profiles are used by six full-wave solver groups to simulate the ICRF electromagnetic fields and heating, and by three of these groups to simulate the current-drive. Approximate agreement is achieved for the predicted heating power for the DT and He<sup>4</sup> cases. Factor of two disagreements are found for the cases with second harmonic He<sup>3</sup> heating in bulk H cases. Approximate agreement is achieved simulating the ICRF current drive.

pacs: 07.05.Tp, 28.52.Av, 28.52.-s, 28.52.Cx, 52.55.Fa

## 1. Introduction

Ion-cyclotron range of frequency (ICRF) heating will be an important component of the ITER heating system. The planned heating power is up to 20 MW and the range of frequency is 40-55 MHz. Simulations of ICRF heating current-drive, and torque profiles are needed for estimating the effectiveness of the ICRF system in helping to create and sustain high fusion power. To get realistic plasmas for ICRF simulations and for performance predictions, integrated modeling is needed since the plasma profiles and applied heating are strongly coupled. Benchmarking of the codes used for simulating the heating is important for verifying and assessing confidence in the simulations and in the predictions.

Time-dependent integrated modeling needs to balance physics fidelity and numerical resolution with run speeds. Simulating some ICRF effects such as mode conversion, and some plasma regimes require much greater spatial resolution than others. Hence an important byproduct of benchmarking is an indication of the numerical resolution needed for accurate full-wave simulations, and also of the level of model sophistication needed to capture the important physics.

Several phases of plasma operation are planned for ITER. ICRF scenarios are discussed in Ref [1]. A pre-activation phase is scheduled for checking, testing, and calibrating the heating, diagnostics, stability, control, fueling, exhaust, and safety systems. It will be especially helpful if the H-mode can be obtained in this phase for studying first wall heating, ELM effects, and disruption control. There are indications that the H-mode might be achieved in hydrogen and He<sup>4</sup> - dominated plasmas with low field and density, and with the planned auxiliary heating power.

The auxiliary heating and current-drive systems being designed for both the pre-activation and initial DT phases are negative-ion neutral beam injection (NNBI), ICRF, and electron-cyclotron range of frequency (ECRF). NNBI simulation codes have been extensively benchmarked for present experiments and for ITER [2, 3]. Likewise ECRF simulations have been benchmarked in present experiments and in ITER [4]. ICRF simulation codes have been benchmarked using profiles from existing experiments, but have not been thoroughly benchmarked for predicted ITER plasmas. The purpose of this paper is to benchmark the full-wave solvers used for ICRF simulations.

## 2. Benchmark cases

The PTRANSP code [5–8] is used to generate predictions of ITER plasmas for use as benchmarking cases. The cases are listed in Table I. The PTRANSP predictions are time-dependent, integrated, and self-consistent in that the heating, current-drive, and beam torques are calculated using predicted plasma profiles. The up/down asymmetric geometry of the flux surfaces is included. An example is shown in figure 1.

The cases include a high performance baseline ( $B_{TF}=5.3$  T,  $I_p=15$  MA) DT plasma (case 1), and plasmas for the pre-activation phase with half-field and half-current plasmas with either bulk H (cases 2 and 3) or He<sup>4</sup> (case 4). The DT case 1 is taken from Ref [7]. Case 2 is in L-mode and the others are in H-mode. For the pre-activation bulk H cases the dominant absorption of ICRF power is via electron Landau damping (ELD), second harmonic heating of the He<sup>3</sup> minority with frequency twice the ion-cyclotron frequency ( $\omega = 2\Omega_c$ ), and first harmonic heating of the majority H ( $\omega = \Omega_c$ ). The second harmonic heating fraction is calculated to increase by increasing either the density or the energy of the He<sup>3</sup>. Since case 2 is predicted to be in L-mode, the NNBI power is raised from 17 to 33 MW for case 3. Also the fraction of He<sup>3</sup> is raised from  $n_{min}/n_e$  of 0.03 to 0.20. This case is predicted to be marginally in H-mode. Both increases result in increased He<sup>3</sup> heating.

Cases 2 and 3 (accelerating He3 at its second harmonic) are numerical explorations of a heating scenario under assessment but currently not considered a main scenario for ITER. Experiments with this scheme using low concentrations of He<sup>3</sup> have been conducted in JET [9] and Tore Supra [10]. The results have not been encouraging. In JET either low electron density (conductive to tail formation) or high He<sup>3</sup> concentrations ( $\geq 15\%$ ) are needed in order to see increases in the ion temperature. Perhaps the heating power in these experiments was not sufficiently high to achieve high He<sup>3</sup> energies.

Another pre-activation scenario is case 4 with H minority at half-field in a bulk He<sup>4</sup> plasma with fundamental absorption at 42 MHz. One rationale for this case is that it could be important for obtaining H-mode in the pre-activation phase, especially if the H-mode cannot be achieved in bulk hydrogen. Scalings for the L→H power threshold in He<sup>4</sup> plasmas are controversial, but some tokamaks report lower H-mode threshold in He<sup>4</sup> than in H [11]. The predictions achieve H-mode with extrapolations of database results for  $P_{LH}$  [12]. Also, this case appears to be relatively easy for benchmarking since indications are that this case will have strong single-pass absorption and will not have strong mode-conversion (which is not treated in some of the codes involved in the benchmarking).

The PTRANSP outputs, used as inputs for the full-wave solvers are the plasma equilibria and profiles of the densities and temperatures of the thermal plasma (including impurities) and fast ion species. The predicted plasma profiles are provided for the full-wave codes in the format of "plasma state" netcdf files. The equilibria inputs are provided as "g-eqdisk" files. An alternative set of ASCII input files are provided, with the equilibria in the form of Fourier poloidal moments specifying the (R,Z) values of constant magnetic flux surfaces.

Perpendicular and parallel energy densities of the minority, beam, and fast alpha ions are also specified in both forms. The total perpendicular and parallel energies of the minority ions are given in Table I. Their effective temperatures can be defined using either an isotropic profile:

$$T_{iso} = 2/3 \cdot (e_{\perp} + e_{\parallel}) / (n_{fast} \cdot Z_{fast} \cdot e), \quad (1)$$

or two anisotropic profiles:

$$T_{\perp} = e_{\perp} / (n_{fast} \cdot Z_{fast} \cdot e), \quad T_{\parallel} = 2 \cdot e_{\parallel} / (n_{fast} \cdot Z_{fast} \cdot e), \quad (2)$$

where  $n_{fast}$  is the fast ion density and  $Z_{fast} \cdot e$  is the fast ion charge. Profiles of the thermal ion and electron temperatures  $T_i$  and  $T_e$  and of  $T_{\perp}$  and  $T_{\parallel}$  for the minority ions are shown in figures 2. Note that relatively large "tail" temperatures and large differences between  $T_{\perp}$  and  $T_{\parallel}$  are predicted.

The benchmark cases assume a simple toroidal spectrum for the ICRF at the antenna. For most of the results one wavenumber is used with  $n_{\phi} = \pm 27$ , (symmetric in  $\phi$ ). For current drive simulations only one peak is assumed. This wavenumber corresponds to  $k_{\phi} = 4.229 \text{ m}^{-1}$ . The equivalent parallel

index is 3.843. Different approximations for the antenna, scrape off, and vacuum vessel are assumed by the different wave-solvers. More details about the assumptions used in PTRANSP are given in [Appendix 1](#).

### 3. Full-wave solvers

The profiles and equilibria predictions are used independently by six groups to simulate the ICRF electromagnetic fields and plasma heating. The codes include AORSA [13, 14], CYRANO [15, 16], EVE [17], PSTELION [18], TASK/WM [19], and TORIC (version 6) [20, 21], (version 5 is used for the PTRANSP-generated inputs for the simulations). A summary of approximations and numerical methods is given in [Table II](#). Except for AORSA, all the codes are very similar. EVE has a different formulation of the wave equations. Some codes do not describe mode conversion. TORIC and PSTELION do. There are different choices of which distribution functions can be used to calculate the wave-equation coefficients: mono-Maxwellian (Eq. 1), bi-Maxwellians (Eq. 2), or a numerical distribution.

Parameters needed for quantitative comparisons of the benchmarking results include the locations of resonance layers, zero-dimensional results such as the heating partitions, one-dimensional results such as heating profiles and electromagnetic fields along chords. Two-dimensional contours of heating and electromagnetic fields are very useful for giving insight about the solutions, and to check that the geometry and plasma profiles are being read in correctly by the full-wave solvers, but they do not lend themselves easily to quantitative comparisons. It is important to check the locations of resonance layers since which locations are inside the plasma are complicated by the general shape of the boundary, and by the fact that in time-evolving simulations the boundary shifts.

Part of the research for this benchmarking involved refining and standardizing methods for inputting data to the full-wave solvers. Besides being important for the benchmarking comparisons, the ability to read numerical equilibria and fits to data are important for testing the solvers with experimental data. More details about the full-wave solvers are given in [Appendix 2](#).

### 4. Fokker-Planck solvers

The minority heating and phase space distributions need to be predicted for accurate simulations. This is especially complicated in scenarios where the fast ions are resonant with the ICRF. In such cases, and also if finite orbit effects are important, Monte Carlo techniques appear necessary for accurate coupling of the wave heating, but Monte Carlo techniques are very challenging, especially in the presence of multiple fast-ion species. Various Fokker-Planck codes have been coupled to full-wave solvers. These can have complications of averaging over banana orbits and loss of Finite Larmor Radius (FLR) effects.

The Fokker-Planck module in PTRANSP (FPPRF) uses the up/down asymmetric equilibria, and the bi-Maxwellian assumption Eq. 2. Results for the predicted minority temperatures are shown in [figures 2](#), and results for the ICRF and minority heating of the thermal plasma are given in [Table III](#). The CQL3D Fokker-Planck solver [22] which can be run with AORSA can compute the phase space distribution in energy and pitch angle using up/down symmetric equilibria. Although benchmarking of the Fokker-Planck modules is not part of this paper, AORSA-CQL3D simulation results are included for comparisons with PTRANSP-FPPRF.

### 5. Benchmark results

The locations of the resonance surfaces can depend sensitively on the ICRF frequency. The locations computed by PTRANSP are given in [Table IV](#). The locations of the ion-ion resonances and ion-ion-cutoff for cases 1 and 4 are given in [Table V](#). These locations agree approximately with those found by the full-wave solvers. The heating power partition among the plasma species depends sensitively on details such as the density and effective temperature of the minority ions. Results for the direct ICRF heating from the full-wave solvers for case 1 are shown in [Table VI](#). The heating partitions for the ion species are in approximate agreement. The partitions for direct ICEF-electron heating are in the range 14-39%, so the total ion heating dominates. The partitions for impurity and fast ion species are small. Results for the heating partitions for the pre-activation case 4 in bulk He<sup>4</sup> plasma are also in approximate agreement, as shown in [Table VII](#). Again, the total ICRF-ion heating dominates.

Plots of the real and imaginary parts of various components of the oscillating electric field along the major radius are shown in [figure 3](#). Two cases are compared: case 1 with 10 MW ICEF and case 2 with 20 MW at the benchmark time. The ICRF E and B fields scale with the square root of the power. The results for case 1 indicate strong single-pass absorption since the magnitudes of the simulated fields are relatively small inboard of the minority resonance near the magnetic axis ([Table IV](#)). Similar results are seen for case 4, the other case with first-harmonic minority heating. Mode conversion to propagating Ion Bernstein Waves IBW is negligible for the DT case 1, as indicated by the absence of rapid radial oscillations in plots of the real and imaginary parts of E(R) [figure 3-a](#)). This reduces the requirement of high numerical resolution. Simulations with the resolution increased beyond certain values produce nearly identical results, indicating the minimal resolution required for accuracy.

In contrast to case 1, weak single pass absorption is simulated for case 2 since the magnitudes of the fields are relatively large inboard of the magnetic axis. Qualitatively similar results are seen for both second harmonic minority heating cases. This makes the numerical solutions much more challenging since second harmonic heating is a FLR effect. Plots for the real and imaginary parts of E(R) for case 2 shown in [figure 3-b](#)) indicate that single pass absorption is weaker, and that mode conversion to propagating IBW's is negligible. Heating partitions for cases 2 are listed in [Table VIII](#). The majority of the direct ICRF heating via damped IBW's is indicated. A wide variation is found for the heating partition to the thermal H and He<sup>4</sup> ions. Heating partitions for case 3 are listed in [Table IX](#).

The differences among the full-wave simulations for case 2 could be due to inadequacies in the treatment of the minority species, to lack of numerical convergence of the wave-solvers, or to breakdown of the FLR approximation. The perpendicular and parallel energy densities of the minority ions specified for the wave-solvers are evolved in PTRANSP by FPPRF and input by the full-wave solvers as effective tail temperatures. The AORSA-CQL3D result (using CQL3D for the minority distribution) is shown for comparison in the Tables. It is known that use of effective Maxwellian distributions are adequate for fundamental resonance heating [[23](#), [24](#)], but can over-estimate the high energy tail for cases with second harmonic absorption. This can get exaggerated as TORIC iterates with FPPRF. CQL3D can predict the He<sup>3</sup> phase-space distribution including the second harmonic He<sup>3</sup> cyclotron damping without assuming a form for the minority velocity distribution. The results in [Table VIII](#) show large differences between PTRANSP-FPPRF and AORSA-CQL3D, and even between AORSA-CQL3D and AORSA-iso. The source of these differences is under investigation. Closer agreement is found for case 3, shown in [Table IX](#).

On the other hand the TORIC-FPPRF and AORSA-CQL3D predictions for fundamental absorption in the cases 1 and 4 are much closer, suggesting the simpler treatment of fitting the energetic tail to mono or bi-Maxwellians may be a better approximation for the stronger single pass fundamental minority heating cases, or that the FLR approximation used in the full-wave solvers (except for AORSA) is more accurate than for the 2<sup>nd</sup> harmonic scenario.

Contours of components of the electric field are shown in [figure 4](#) and [figure 5](#). These show approximate agreement for the full-wave solutions, and confirm the weak-single-pass absorption shown in [figure 3](#). Contours of ICRF heating for case 1 are shown in [figure 6](#). The heating simulations required for use in present state-of-art transport codes are flux-surface averaged profiles. Simulations of direct ICRF-heating profiles for case 1 are shown in [figures 7](#). Approximate agreement is found for most of the benchmark full-wave solvers. The PTRANSP results, shown in [figures 7-f](#)), are less peaked, apparently due to the use of a coarser grid.

Profiles of ICRF-driven currents are also needed for realistic modeling. These can be calculated using full-wave solvers coupled to Fokker-Planck solvers, or by using the Ehst-Karney [[25](#)] formula. Examples calculated by three of the full-wave solvers using this formula are shown in [figures 9](#). The results from AORSA-iso are similar to results from AORSA-CQL3D (not shown). The flux-surface (area-integrated) currents are also shown. The currents simulated for the pre-activation cases (with half current) are two to six times that for the DT case 1. For case 2 the total ICEF-driven current RFCD is 0.7 MA which is significant compared the total plasma current of 7.5 MA, so effects on the q profile could be significant, and RFCD could be useful for controlling the current. The results from EVE and TORIC for case 1 are also shown. The total simulated currents are slightly higher than that in [figures 9-a](#)). The TORIC peak current profile near the axis in [figures 9-f](#)) is higher by a factor of 2.5. These differences

could be due mainly to differences in grid resolution. The total RFCD currents are comparable to those in [figures 9](#). The indirect plasma current drive from the minority ions is not included.

## 6. Results for variations of the cases with reduced minority concentrations

There are several motivations for extending the studies to cases for which the minority fractions are reduced. For instance, the cost of  $\text{He}^3$  is very high so routine use at high concentrations might be unacceptable. Variations in the fraction of minority species are studied with some of the full-wave solvers. The results for the heating partitions for case 1 are in general agreement with the fraction of tritium heating increasing to  $\simeq 40\text{-}50\%$  and the fraction to the minority decreasing to low values as the fraction of minority ion density decreases. Comparisons of the heating partitions with an alternative assumption of low  $\text{He}^3$  fraction are given in [Table X](#). It is interesting to note that the electron absorption for the two cases is about the same, but that the T power is reduced by about the same amount as the  $\text{He}^3$  minority increases. Since some of the  $\text{He}^3$  minority power is deposited on the electrons (via slowing down), it appears that no  $\text{He}^3$  would offer a little more direct ion heating than the minority case.

## 7. Grids and convergence

Various checks indicate how well converged the solutions are. A test of global power balance is given by comparing the  $\mathbf{J} \times \mathbf{E}$  loading of the antenna, the Poynting flux through the plasma surface, and the total power deposited in the plasma. Another check is given by comparing the radial oscillations with the grid spacing.

Initial AORSA runs were conducted at a resolution of  $128 \times 128$  (in cylindrical R,Z space) for the Fourier basis sets. These results were checked at a higher resolution of  $256 \times 256$ , with little change in the results. Runs for the higher resolution required  $\simeq 1000$  processor hours (e.g. 1 hour on 1024 processors), while the lower resolution runs required  $\simeq 4^3$  less resources (a few minutes at 512 processors) ( $n^3$  in the resolution).

The TORIC simulations are well-converged with 63 poloidal modes and 403 radial zones. The convergence as the grid resolution is refined is indicated in [Table XI](#). The TORIC convergence is discussed in more detail in [Appendix 2.6](#).

## 8. Discussion and conclusions

The benchmarking simulations find only small heating partitions to the impurity and fast ion species. This suggests that simulations might obtain accuracy without including many species. Numerical convergence for case 1 is studied using AORSA, EVE, and TORIC. Results show that good convergence in the solutions is achieved with grids compatible with integrated, time-dependent prediction codes. Comparisons of the assumptions of mono-Maxwellian versus bi-Maxwellian minority temperatures are done using EVE for all four cases. The results show small (few%) effects in the heating fractions. The effects of including the up/down asymmetry for case are studied using PSTELION, which uses either a symmetric or an approximate up/down asymmetric geometry. Differences for the heating are small.

The benchmarking of full-wave solvers for the fundamental harmonic cases 1 and 4 give similar results, indicating that the solutions should be reliable. One question concerning Case 4 is whether mode-conversion plays a significant role with 20%H. If the radial / poloidal grid is sufficiently coarse the simulation will not capture the short wave structure. It is not clear if the MC is really not efficient because of the large gap between the FW cut-off and the MC layer in this case.

Results for the pre-activation second harmonic cases 2 and 3 with bulk H have larger differences. Consistent amongst the different codes but very sensitive to small changes in the plasma / RF parameters. Because of its low absorptivity there is a large component of 'sloshing-around' reactive power and the different  $k_{\parallel}$  components of the antenna spectrum behave very differently. Probably a single  $k_{\parallel} = N/R$  calculation is indeed representative of the 'real' power absorption in this case. These cases might not be useful for ITER due to the cost of  $\text{He}^3$ . The convergence of the full-wave solutions needs to be examined in more detail. Better solutions of the minority distributions are needed.

Issues that need to be explored further are: 1) effects of including a more realistic  $n_\phi$  spectrum. In cases where the absorption computed using a simple spectrum is weak, a more realistic antenna model and spectrum would allow for distortion of the spectrum by the plasma and could result in stronger absorption; 2) improved simulations of the minority distribution and plasma heating. For accurate simulations in transport codes both the direct ICRF and the minority heating are needed.

#### **Acknowledgments**

We wish to thank P. Lamalle, A. Polevoi, and J. Snipes for helpful suggestions and comments. This work is supported in part by the US DoE Contract No. DE-ACO2-76-CHO3073.

### Appendix 1 - PTRANSP predictions of the benchmark cases

The PTRANSP code [5–8] is used to generate predictions for the plasma conditions. The predictions are integrated and self-consistent in that the heating, current-drive, and beam torques are calculated using predicted plasma profiles. Several physics effects not yet included are the ICRF-induced and intrinsic rotation. The heating, neutral-beam-torquing, and current drive profiles are used in the local flux-averaged energy, momentum, and magnetic field balance equations, and the time-evolution of the temperature and minority distributions are predicted. The up/down asymmetric geometry of the flux surfaces are included. An example is shown in figure 1. The temperatures are calculated using GLF23 [26] and a pedestal model [27] incorporated into PTRANSP which predicts the pedestal pressure. The boundary values for GLF23 are the temperatures at the top of the pedestal. Temperature profiles are shown in figures 2. For case 1 the toroidal rotation profile (needed for the flow shearing rate) is calculated assuming that the ratio of momentum to ion energy transport is 0.05. For the other cases GLF23 is used to also compute self-consistently the toroidal rotation.

The PTRANSP runs typically use several hundreds of hours of CPU with about one-third of the CPU are used for TORIC (version 5) with a low number of poloidal modes (31). The runtime increases as the cube of the number of poloidal modes, so increased accuracy requires much more CPU.

The auxiliary heating for the DT case 1 is assumed to start with 73 MW (the total planned for ITER), since the maximum may be needed to induce the transition to a high-performance H-mode. This power is composed of 33 MW of D-NNBI at 1 MeV, 20 MW ICRF, and 20 MW ECRF. The heating is stepped down as the alpha heating increases, thereby allowing the fusion gain  $Q_{DT}$  defined as the ratio of the fusion yield over the auxiliary and Ohmic powers to increase. The heating power evolutions are shown in figure 11-a). The  $Q_{DT}$  evolution is shown in figure 11-b). The assumed thermal ion species are D, T, He<sup>4</sup> ash, Be, and Ar impurities; the fast ion species are D-beams, and alphas. The electron density  $n_e$  is assumed to be flat, and the Be and Ar densities are assumed to be  $n_{Be} / n_e = 0.02$  and  $n_{Ar} / n_e = 0.0012$ . The gas fueling, recycling, and ash transport is described in [7]. The plasma has  $Q_{DT} \simeq 12$  at the benchmarking time (245s).

The pre-activation plasmas are assumed to have a shorter duration with the  $n_e$  profile ramped up to a peak of  $4.6 \times 10^{19} m^{-3}$  by 80 s. The profile is assumed to be flat. ICRF heating of 20 MW and ECRF heating of 20 MW are assumed to start at 50 s. For the bulk H cases 2 and 3 the H-NNBI is assumed to be 17 and 33 MW respectively. The evolutions of the heating powers are shown in figure 11. The beam voltage is assumed to be 870 keV to avoid excessive power shine-through. The impurity is assumed to be only C with density 2 % of  $n_e$ . GLF23 is run in the “option 2” mode discussed in [8] with the toroidal rotation and flow-shearing rate profiles computed by GLF23. This results in predictions achieve moderately high central temperatures even with low pedestal temperatures.

Recent extrapolations of database values of the L→H power threshold scalings of the H-mode threshold, [12])

$$P_{MW} = 2.15 \kappa^{\pm 0.107} n_{e20}^{0.782 \pm 0.037} B_{tesla}^{0.772 \pm 0.031} a_m^{0.975 \pm 0.08} R_m^{0.999 \pm 0.01} 2.0 / MAMU \quad (3)$$

indicate that the case with 17 MW will not achieve the H-mode (figure 11-c)), but with 33 MW will (figure 11-e)). The threshold power increases with density and toroidal field, so lower density and toroidal field are preferable. Comparisons of the predicted volume-integrates thermal ion and electron heat depositions and the scaling are shown in figure 11-d). For this reason, case 3 is also considered with two beamlines delivering 33 MW of H-NNBI. This case appears to access the H-mode (barely) using [12].

Both the full field DT and half-field bulk H cases use the ICRF frequency of 52.5 MHz, and assume the minority ion species is He<sup>3</sup> at a density relative to the electron density of 2% for the DT and 3% for the pre-activation case. The He<sup>3</sup> absorption is at the fundamental frequency for the DT case and at the 2<sup>nd</sup> harmonic for the half-field case. He<sup>3</sup> heating is of interest for achieving a significant partition of the heating to thermal ion species, but it is considered optional for ITER. The ion partition increases with increasing He<sup>3</sup> density, but high He<sup>3</sup> density would dilute DT fuel. Also achieving large concentrations of He<sup>3</sup> in the resonance layer appears to be far too expensive for routine use. Another

concern is that having a large partition of the heating to fast ion species may be undesirable due to causing excessive losses and TAE drive.

The scalings for the L→H power threshold in He4 plasmas is controversial. The GLF23 predictions achieve H-mode with the Martin scaling. Predicted temperature profiles are shown in [figure 2-d](#)). The minority ions also heat the electrons and thermal ions, and the accumulated heating for case 1 is shown in [figure 12](#). Note that the minority heating can be negative at large radii due to the plasma heating the minority instead of the expected vice-versa. Also the minority heating can be significantly larger than the ICRF heating, as in the case 4 electron heating. Only case 1 is predicted to have approximately equal total ion and electron heating. The importance of including the plasma heating by the minority ions is shown in [figure 13](#) where the fraction of H minority in the bulk He<sup>4</sup> case 4 is scanned. Although the direct RF-electron heating increases as the H concentration increases, the H heating of electrons decreases.

A simplified antenna is used for the PTRANSP predictions. It is assumed to extend poloidally 1.83 m, and is located 0.18 m outside the plasma boundary. The toroidal spectrum at the antenna is approximated by one wavenumber  $n_\phi = 27$ , corresponding to  $k_\phi$  is  $4.229 \text{ m}^{-1}$ . The equivalent parallel index is 3.843. The ITER antenna design is composed of four columns of six short poloidal straps ( $\simeq 0.27\text{m}$ ). The top and bottom triplets of straps are driven in quadrature through an ELM-tolerant 3dB hybrid splitter. The vacuum vessel is assumed to be perfectly conducting, and thus the ICRF excites image currents in the vessel. These have small effects within the separatrix region if the antenna is not placed (numerically) close to the vessel.

## Appendix 2 - Full-wave codes

**2.1 AORSA** - A plasma state file was pre-processed by a wrapper program that was developed for the Simulation of Wave Interactions with MHD (SWIM) project. For the case of energetic species where  $E_\perp$  and  $E_\parallel$  are provided (NUBEAM for NNBI ions and fusion products, FPPRF for minority) and an isotropic effective temperature given by [Eq. 1](#) was used. Because of internal limitations for AORSA, only six species could be used. For the initial DT case 1 these are assumed to be electrons, T, D, He<sup>4</sup> ash,  $D_{nb}$ , alpha particles, and He<sup>3</sup> minority. Of these only electrons, T, and He<sup>3</sup> min were significant. The  $D_{nb}$  and alpha particles, were replaced with the Ar and Be. The RF power in these species was small. Thus the plots only show electrons, T, and He<sup>3</sup> minority for clarity.

AORSA can be run with CQL3D, providing the possibility to model the minority distribution self consistently. Previous ITER simulations with AORSA (e.g. [\[13, 14\]](#)) used this mode. The ITER benchmarking cases were run both in this mode and using the effective isotropic temperature derived from the PTRANSP-FPPRF inputs. The CQL3D work can be done by interacting several times between AORAS and CQL3D. The results using FPPRF or CQL3D are very close.

The present work uses one toroidal wavenumber ( $n_\phi = 27$ ) to model the antenna current. Analysis using a full spectrum can also done (cf reference above). For these calculations several tens to 50 runs are required.

For the 2D version used for this study, the antenna is a current strap just inside the last closed flux surface, with a  $\cos(ky \times y)$  profile for the current, where  $ky = k_0 \times \text{antlc}$ , and antlc is a specified propagation constant, exactly as in TORIC. In a new version being developed the antenna can be outside the last closed flux surface. In 3D, with the full antenna spectrum, the antenna is some number of step function currents (4 for ITER, 12 for NSTX) with a given phasing between them. For the 2D version used for this study, the region between the antenna and plasma is not modeled separately, but is whatever the profiles give for that region up to  $x = 1$ .

Results for the heating partitions are given in [Table VI](#). Comparisons of the heating partitions with an alternative assumption of low He<sup>3</sup> fraction are given in [Table X](#).

**2.2 CYRANO** - The CYRANO code was developed by Lamalle [\[15\]](#), and is very similar to TORIC. It uses finite elements in the radial direction and Fourier representation in the poloidal and toroidal dimensions. It only treats axi-symmetric equilibrium so toroidal modes are independent, and solves the wave equation in the weak variational form ('Galerkin formalism'). The antenna model is

idealized: infinitely thin straps in the radial direction, homogeneous antenna currents, includes radial feeders. The dielectric tensor includes corrections up to  $2^{nd}$  order Larmor radius. It has been modified to include general (numeric) distribution functions to compute the dielectric response [16], and coupled to the quasi-linear Fokker-Planck code BATCH [28] to self-consistently model the RF acceleration / quasi-linear diffusion problem. This has been successfully tested for fundamental ( $N=1$ ) heating of NBI ions in JET [16].

CYRANO is non-Parallel and runs on one (quad-core) CPU. The results shown here 200 radial points x 128 poloidal modes are used. Results for the heating partitions are given in Table VI. Comparisons of the heating partitions with an alternative assumption of low He<sup>3</sup> fraction are given in Table X.

**2.3 EVE** - The EVE code [17] is a full-wave solver based on a variational formulation of the Maxwell-Vlasov system. The wave particle interaction is described by a quasi-local plasma functional, in which a first order expanded version of the particle Hamiltonian has been implemented. The quadratic dependency of the functional on the interaction Hamiltonian makes of EVE a second-order FLR code. The use of a Hamiltonian formulation and associated action-angle variables has the advantage of providing a common framework to the wave and the quasi-linear response calculation, making EVE the main element in a wave + kinetic package.

The core of the code is written in Fortran 90, parallelized, and runs on various clusters and supercomputers. It also features a post-processor written in Python. It is based on a toroidal geometry and can read analytical, HELENA, EFIT, or ITM equilibria. The plasma profiles may be specified analytically, point-wise or read from the ITM data tree. The four cases are simulated with the effective temperatures taken as either isotropic Eq. 1 or anisotropic Eq. 2. Also the four cases were simulated assuming that the minority temperature equals the thermal ion temperature, i.e., that the plasma does not have an ICRF-heated tail.

Release version 1.4.7 is used for the results here. The grid used 460 radial and 512 poloidal points and 129 poloidal modes. The antenna is located between 8.38 and 8.39 m, with feeder locations specified. The provided EFIT equilibrium and TRANSP profiles have been directly used. Results for the heating partitions are given in Tables VI-X. Comparisons of the alternative assumptions of isotropic or anisotropic-Maxwellians for the minority temperatures are shown in Table XII.

**2.4 PSTELION** - The code has two versions: STELION1 AND PSTELION. PSTELION is a newly developed stellarator ICRF 3D full wave code based on theory described in reports [18],[29]. The code solves wave excitation, propagation and absorption in 3D stellarator equilibrium high beta plasma in ion cyclotron frequency range and lower. The Maxwell-Vlasov boundary value problem at the ICRF frequency range is solved on realistic equilibria in an elongated toroidal plasma geometry (produced by equilibrium solver as, for example, VMEC code [30]). This code is useful for ICRF heating scenarios development.

The code solves the 3D Maxwell-Vlasov antenna-plasma conducting shell boundary value problem in non-orthogonal flux coordinates  $(\Psi, \Theta, \phi)$  with  $\Psi$  being the magnetic flux function,  $\Theta$  and  $\phi$  being the poloidal and toroidal angles, respectively. All basic physics, like wave refraction, reflection, diffraction and Mode Conversion (MC) are self consistently included, along with the fundamental and second harmonic ion and ion minority cyclotron resonances, two ion hybrid, Alfvén resonances, ELD and TTMP absorption. This is accomplished in a real confining magnetic field in a plasma major radius direction, in toroidal and poloidal directions, through making use of ion and electron FLR effects in wave plasma response second order differential operators. In the Reduced Order Algorithm code option the hot plasma the dielectric kinetic tensor is used (FLR effects are accounted through reduced order scheme).

The numerical methods use an expansion of the solution in Fourier series over  $\phi$  and  $\Theta$  angles and solves resulting ordinary differential equations in a radial like  $\Psi$  coordinate by finite difference method. The constructed discretization scheme is divergent free one, thus retaining the basic properties of original equations. The Fourier expansion over angles coordinates allows a correct construction of the parallel wavenumber  $k_{\parallel}$  and thereby correctly describe the ICRF waves absorption by a hot plasma. The toroidal harmonics are tightly coupled with each other due to magnetic field inhomogeneity of stellarators in toroidal direction. The code is developed in a manner that includes tokamaks and

mirrors as the particular cases through general metric tensor (provided by a plasma equilibrium solver) treatment of the wave equations. The resulting system of linear equations is solved by making use the ScaLAPACK library of parallelized linear algebra routines and direct use of the MPI interface.

STELION1 and PSTELION are coupled with 2D STIION Fokker-Planck code [29] which uses flux surface averaged RF absorbed specific power in quasi-linear diffusion operator to calculate the minority ions distribution functions on chosen magnetic surfaces. The application of the code to stellarators is also given in attached paper [5] in report [5]. Calculations requiring a large number of Fourier harmonics generate very large matrices. While these can be written to disk (for some particular sparse matrix solvers) when necessary and subsequently retrieved as required, this increases the computer time substantially. The calculations with STELION1 (no mode conversion to IBW) on IBM-SP with 16 processors for 3D task problems for the NCSX plasma with  $NPSI = 71$ ,  $NTHETA = 64$ ,  $NZETA = 8$  has shown necessity about 1.3 GB of RAM and calculation time about 3 hours for CPU at 1.3 GHz. Doubling the number of poloidal or toroidal modes leads to increase of CPU time about 5 times. PSTELION code operating on terabyte massive computers includes mode conversion processes and CPU requirements are more severe ones.

PSTELION was built to use an up/down symmetric equilibrium. It was recently generalized to approximate up / down asymmetric equilibria using the VMEC2000 solver. Results for the heating partitions from the up / down asymmetric case are given in Table VI. A comparison of results with alternative assumptions up/down symmetric and asymmetric magnetic flux geometry are given in Table XIII.

**2.5 TASK/WM** - TASK/WM solves Maxwell's equations as a boundary value problem with magnetic flux coordinates in 3D configuration. Fourier mode expansion in poloidal and toroidal directions, and finite element method in radial direction are used. Various kinds of dielectric tensors for any number of particle species can be used. The kinetic dielectric tensor includes the the plasma dispersion function. Finite Larmor radius effects are included as a fast wave approximation. TASK/WF is coupled with Fokker-Planck code TASK/FP and orbit code GNET. The dielectric tensor for arbitrary velocity distribution function is treated in TASK/DP. Results for the heating partitions for the DT case 1 are given in Table VI.

Future work is 1) arbitrary antenna configuration, 2) Finite Larmor radius effects in a integral form, 3) Coupled with Fokker-Planck code, 4) parallel processing with TASK/WM/FP/DP.

**2.6 TORIC** - TORIC [20, 21] solves Maxwell's equations in axisymmetric toroidal plasmas, assuming a constitutive relation (linear relation between high-frequency field and high-frequency plasma current) obtained from the linearized Vlasov equation by expanding the wave field in toroidal and poloidal Fourier components. The model includes propagation and damping of externally launched fast waves (FW), as well as of Ion Bernstein (IBW) and Ion Cyclotron (ICW) waves excited by linear mode conversion (LMC) near ion-ion resonances. The absorption channels are fundamental and first harmonic IC heating of ions, and ELD and Transit Time damping of electrons. Optionally, damping of the FW at higher IC harmonics can be simulated [31]. The coefficients of the wave equations are evaluated for arbitrary distribution functions using the information transmitted from the Fokker-Planck package SSFPQL [32]. Recent applications of the TORIC code can be found in [33]

The version 6 used for the benchmarking uses a new algorithm (originally invented for the numerical solution of the wave equations in the Lower Hybrid frequency range) has been implemented in the vacuum region surrounding the plasma. It allows to solve Maxwells equations exactly and with the same cubic finite elements as in the plasma, yet completely avoiding numerical pollution. As a result, the global power balance (agreement between the  $J \times E$  loading of the antenna, the Poynting flux through the plasma surface, and the total power deposited in the plasma) is often appreciably more accurate than in previous TORIC versions. Thus in the preceding examples this agreement, which is a reliable indicator of convergence, was better than 0.3%, in spite of the fact that, in order to execute on a laptop, only 128 points were used in the poloidal mesh, and thus only 63 poloidal Fourier modes in the representation of the fields. A further indication of convergence was the fact that the results did not significantly differ from those obtained with only 64 points and 31 Forier modes, whose power balance was only marginally less accurate.

Results for the heating partitions for the DT case are given in [Table VI](#). A comparison of results with alternative assumptions for the number of poloidal modes and radial grid are given in [Table XI](#). Results for pre-activation case - A strong sensitivity to the He<sup>3</sup> energy is found. The results with elevated He<sup>3</sup> energy are the same as from PTRANSP.

The Fokker-Planck package SSFPQL [\[34\]](#) evaluates the steady-state quasi-linear distribution function of ions heated at the fundamental and first harmonic IC resonance by balancing the bounce-averaged quasi-linear operator (QLO) with the linearized collision operator describing collisions with a Maxwellian background plasma. The solution is obtained as a truncated series in Legendre polynomials. A special Bessel function identity is used to guarantee that the truncated Legendre expansion of the QLO remains positive definite up to sufficiently high energies. This approach does not allow to deal with the most energetic ions generated by IC resonances, or to follow transients when the hf power is switched on and off or modulated in time. Nevertheless, with some further limitations discussed in [\[32\]](#), most of them common to all kinetic equations based on surface averaging, the information provided by SSFPQL on the radial profiles of the quasi-linear distribution functions are fully adequate for the purpose of evaluating the coefficients of the wave equations for iteration with the wave solver.

- 
- [1] Gormezano, C., Sipps, A.C.C., Luce, T.C., Ide, S., *et al.*, Nucl. Fusion **47** (2007) S312.
  - [2] Houlberg, W.A., Gormezano, C., Artaud, J.F., Barbato, E., Basiuk, V., *et al.*, Nucl. Fusion **45** (2005) 1309.
  - [3] Oikawa, T., *et al.*, 22th IAEA Conference, Geneva **IT/P6-5** (2008).
  - [4] Prater, R., Farina, D., Gribov, Y., *et al.*, Nucl. Fusion **48** (2008) 035006.
  - [5] Budny, R.V., Andre, R., Bateman, G., Halpern, F., Kessel, C.E., *et al.*, Nucl. Fusion **48**, (2008) 075005.
  - [6] Halpern, F.D., Kritz, A.H., Bateman, . G., *et al.*, Phys. Plasmas **15** (2008) 062505.
  - [7] Budny, R.V., Nucl. Fusion **49**, (2009) 085008.
  - [8] Budny, R.V., submitted to Nucl. Fusion Dec, 2010.
  - [9] Lerche, E., *et al.*, 37th EPS Conf. Contr. Fusion and Plasma Physics, Dublin, June 2010, O4.121
  - [10] Private Communication (2010).
  - [11] Ryter, F., Ptterich, T., Reich, M., Scarabosio, A., Wolfrum, E.,*et al.*, Nuclear Fusion **49** (2009) 062003.
  - [12] Martin, Y.R., *et al.*, Journal of Physics: Conference Series **123** (2008) 012033.
  - [13] Jaeger, E.F., Berry, L.A., Harvey, R.H., Phys. Plasmas **15**, (2008) 072513.
  - [14] Jaeger, E.F., Berry, L.A., Lamalle, P.U., Loarte, A., Polevoi, A., *et al.*, APS DPP, Atlanta, (2009).
  - [15] Lamalle, P., PhD thesis - Université de Mons (1994) LPP-ERM/KMS Laboratory Report 101.
  - [16] Lerche, E., Van Eester, D., Krasilnikov, A., Ongena, J., *et al.* Plasma Phys. Control Fusion **51** (2009) 044006
  - [17] Dumont, R. J., Nucl. Fusion **49**, (2009) 075033.
  - [18] Vdovin, V.L., ICRF benchmarking modelling of ITER scenario No. 2, 7th Steady State Operation ITPA Topical Group meeting, Como, Italy, May 4-6, 2005.
  - [19] Batchelor, D.A., Beck, M., Becoulet, A., Budny, R.V., *et al.*, Plasma Sci. Technol. **9** (2007) 312.
  - [20] Brambilla M., Plasma Phys. Cont. Fusion **41**, (1999) 1.
  - [21] Wright, J.C., Bonoli, P.T., Brambilla, M., Meo, F., *et al.*, Phys. of Plasmas **11**, (2004) 2473.
  - [22] Harvey, R.W. and McCoy, M.G., IAEA Conf. Proc., Technical Committee Meeting on Advances in Simulation and Modeling of Thermonuclear Plasmas (Montreal, Canada, 15-18 June 1998) (Vienna, Austria: International Atomic Energy Agency) p 305.
  - [23] Stix, T., Nuclear Fusion **15** (1975) 737.
  - [24] Hosea, J., Bernabei, S., Colestock, P., Davis, S.L.,*et al.*, Physical Review Lett., **43** (1979) 1802.
  - [25] D. A. Ehst and C.F.F. Karney Nuclear Fusion **31** (1991) 1933.
  - [26] Waltz, R.E., Staebler, G.M., Dorland, W., *et al.*, Phys. Plasmas **4** (1997) 2482.
  - [27] Onjun, T., Bateman, G., Kritz, A.H., and Hammett, G., Plasma Phys. Controlled Fusion **45** (2003) L55.
  - [28] Van Eester D., J. Plasma Physics **65**, p.407 (2001).
  - [29] Vdovin V., The Distribution Function of Resonant Ions at Ion Cyclotron Heating of Plasma in Tokamaks, 2d Grenoble-Varenna Int. Symp. "On Heating in Toroidal Plasmas", (Como 1980), v.1, p.555
  - [30] S.P. Hirshman., J.C.Whitson, Phys. Fluids **26**(12), 3553
  - [31] Brambilla M, Plasma Phys. Cont. Fusion **44**, (2002) 2423.
  - [32] Brambilla M., Bilato R., Nuclear Fusion **49**, (2009) 085004.
  - [33] J. C. Wright, *et al.*, Nuclear Fusion **45**, (2005) 1411.
  - [34] Brambilla M., Nuclear Fusion **34**, (1994) 1121.

| case                          | case 1 (DT)     | case 2 (H)      | case 3 (H)      | case 4 (He <sup>4</sup> ) |
|-------------------------------|-----------------|-----------------|-----------------|---------------------------|
| bulk ion species              | DT              | H               | H               | He <sup>4</sup>           |
| Impurity species              | ash, Ar, Be     | C               | C               | C                         |
| Fast ion species              | D-beam, alphas  | H-beam          | H-beam          | none                      |
| $B_T$ [T]                     | 5.314           | 2.678           | 2.665           | 2.665                     |
| $I_p$ [MA]                    | 15.0            | 7.5             | 7.5             | 7.5                       |
| $n_e(0)$ [ $10^{20} m^{-3}$ ] | 1.05            | 0.46            | 0.46            | 0.46                      |
| $T_i(0)$ [keV]                | 27.5            | 10              | 12              | 13.5                      |
| $T_e(0)$ [keV]                | 25              | 14              | 15              | 12.5                      |
| $T_{ped}$ [keV]               | 5.3             | 1.5             | 2.5             | 1.8                       |
| $\beta_n$                     | 2.0             | 1.5             | 1.8             | 1.2                       |
| $P_{NNBI}$ [MW]               | 17.0            | 17.0            | 33.0            | 0.0                       |
| $P_{EC}$ [MW]                 | 20.0            | 20.0            | 20.0            | 20.0                      |
| $P_{IC}$ [MW]                 | 10.0            | 20.0            | 20.0            | 20.0                      |
| ICRF frequency [MHz]          | 52.5            | 52.5            | 52.5            | 42.0                      |
| minority species              | He <sup>3</sup> | He <sup>3</sup> | He <sup>3</sup> | H                         |
| $n_{minor} / n_e$             | 0.02            | 0.03            | 0.20            | 0.20                      |
| $R_{axis}$ [m]                | 6.392           | 6.320           | 6.475           | 6.419                     |
| $R_{res}-R_{axis}$ [m]        | -1.488 (F1/2)   | -1.368 (F1/1)   | -1.590 (F1/1)   | -0.305 (F1/1)             |
| $R_{res}-R_{axis}$ [m]        | 0.178 (S1/3)    | 0.364 (S2/3)    | -0.096 (S2/3)   | -0.305 (S1/2)             |
| $E_{  }$ (minor) [MJ]         | 1.6             | 0.4             | 3.7             | 3.7                       |
| $E_{\perp}$ (minor) [MJ]      | 3.4             | 1.5             | 10.0            | 9.5                       |

TABLE I: Summary of the benchmarking cases predicted by PTRANSP. Locations of two ion cyclotron resonances (relative to the magnetic axis) are listed along with ratios of  $Z / A$  of ion species with fundamental (F) or second harmonic (S) resonances within the separatrix.

| Code     | FLR                   | Methods   |
|----------|-----------------------|---|
| AORSA    | all orders            | Fourier collocation in $k_x, k_y, k_\phi$                             |
| EVE      | 2 <sup>nd</sup> order | Variation method; toroidal and poloidal modes; radial finite elements |
| CYRANO   | 2 <sup>nd</sup> order | Variation method; toroidal and poloidal modes; radial finite elements |
| PSTELION | 2 <sup>nd</sup> order | Finite differences in radial coordinate                               |
| TORIC    | 2 <sup>nd</sup> order | Variation method; toroidal and poloidal modes; radial finite elements |
| TASK/WM  | 2 <sup>nd</sup> order | toroidal and poloidal modes; radial finite element                    |

TABLE II: Summary of full-wave solvers and their order of Finite Larmor Radii (FLR) approximations and numerical methods used.

| bulk ion species           | DT case 1 | H case 2 | H case 3 | He <sup>4</sup> case 4 |
|----------------------------|-----------|----------|----------|------------------------|
| $P_{ICRF}$ [MW]            | 10.0      | 20.0     | 20.0     | 20.0                   |
| ICRF-electrons [MW]        | 3.7       | 11.1     | 3.9      | 4.0                    |
| ICRF-thermal ions [MW]     | 1.4       | 4.9      | 1.0      | 0.2                    |
| ICRF-minority [MW]         | 5.3       | 4.1      | 15.4     | 16.1                   |
| minority-electrons [MW]    | 1.2       | 1.8      | 10.5     | 10.2                   |
| minority-thermal ions [MW] | 4.0       | 2.3      | 5.2      | 5.5                    |

TABLE III: *PTRANSP-FPPRF* results for heating powers of the ICRF, and for the minority species heating to the thermal plasma. The sums of the last two rows are approximately the total ICRF-minority heating.

| ion species                 | Fund resonance              | 2 <sup>nd</sup> harmonic resonance |
|-----------------------------|-----------------------------|------------------------------------|
| case 1 bulk DT              | axis at 6.385 m             |                                    |
| D                           | -1.488 m                    | 3.437 m (outside boundary)         |
| T                           | -3.111 m (outside boundary) | 0.018 m                            |
| He <sup>3</sup> minority    | 0.018 m                     | 6.711 m (outside boundary)         |
| case 2 bulk H               | axis at 6.320 m             |                                    |
| H                           | -1.368 m                    | 3.721 m (outside boundary)         |
| A/Z=2                       | -3.810 m (outside boundary) | -1.368 m                           |
| He <sup>3</sup> minority    | -2.973 m (outside boundary) | 0.364 m                            |
| case 3 bulk H               | axis at 6.475 m             |                                    |
| H                           | -1.590 m                    | 3.033 m (outside boundary)         |
| A/Z=2                       | -4.098 m (outside boundary) | -1.590 m                           |
| He <sup>3</sup> minority    | -3.306 m (outside boundary) | -0.096 m (outside boundary)        |
| case 4 bulk He <sup>4</sup> | axis at 6.419 m             |                                    |
| He <sup>4</sup>             | -3.401 m (outside boundary) | -0.281 m                           |
| H minority                  | -0.281 m                    | 5.653 m (outside boundary)         |

TABLE IV: Major radii of the magnetic axes for the four cases and the locations of ion resonances measured from the magnetic axis. Ions with the same A / Z ratio have the same locations so, for instance, D beam ions, ash, fusion alphas, and any impurity with ratio 2 have the same as that of thermal D.

| ion species | ion-ion resonance | ion-ion cutoff |
|-------------|-------------------|----------------|
| case 1      | -0.064 m          | -0.084 m       |
| case 4      | -1.076 m          | -0.859 m       |

TABLE V: Locations of the ion-ion resonance layers and the ion-ion cutoff.

| Solver        | T    | thermal D | minority | He <sup>4</sup> ash | electrons  | Ar  | Be  | D-beams | fast alphas |
|---------------|------|-----------|----------|---------------------|------------|-----|-----|---------|-------------|
| PTRANSP-aniso | 12.4 | 0.8       | 49.7     | 0.11                | 36.5 / 0.3 | 0.1 | 0.1 | 0.02    | 0.12        |
| AORSA-iso     | 14.1 | 0.6       | 55.6     | 0.3                 | 29.6       | 0.2 | 0.3 | 0.0     | 0.0         |
| CYRANO        | 18.0 | 1.0       | 41.0     | NA                  | 39.0       | -   | -   | -       | 1.0         |
| EVE-aniso     | 12.5 | 0.4       | 48.8     | 0.1                 | 36.8       | 1.1 | 0.2 | 0.0     | 0.1         |
| EVE-iso       | 12.4 | 0.4       | 48.6     | 0.1                 | 37.0       | 1.2 | 0.2 | 0.0     | 0.1         |
| PSTELION      | 18.4 | 0.1       | 67.0     | 0.02                | 13.6 / 0.6 | -   | -   | -       | -           |
| TASK/WM       | 15.2 | 1.1       | 48.4     | 0.03                | 25.7       | -   | -   | -       | -           |
| TORIC-iso     | 16.0 | 0.5       | 51.2     | 0.03                | 31.7 / 0.7 | -   | -   | -       | -           |
| AORSA-CQL3D   | 13.4 | 0.6       | 56.7     | 0.3                 | 29.3       | 0.2 | 0.3 | 0.0     | 0.0         |

TABLE VI: Comparisons of heating partitions (%) for the case 1 (DT) with  $n_{He^3}/n_e=0.02$ . CYRANO and PSTELION results are for a similar equilibrium. The PTRANSP results are from the runs generating the target profiles. The TASK/WM results are preliminary, for a similar equilibrium and profiles. The PTRANSP-aniso, PSTELION, and TORIC-iso partitions to electrons are split to fast wave and Ion Bernstein Waves (IBW). The AORSA-CQL3D results are for comparison with PTRANSP-aniso and the benchmarking results.

| Code          | H    | electrons    | thermal He <sup>4</sup> | carbon impurity |
|---------------|------|--------------|-------------------------|-----------------|
| PTRANSP-aniso | 78.5 | 20.02 / 0.02 | 1.3                     | 0.1             |
| AORSA-iso     | 81.6 | 17.6         | 0.7                     | 0.07            |
| CYRANO-iso    | 75   | 25           | 2.0                     | <0.1            |
| EVE-aniso     | 73.7 | 25.2         | 1.0                     | 0.1             |
| EVE-iso       | 77.5 | 21.1         | 1.3                     | 0.1             |
| TORIC-iso     | 78.3 | 20.3 / 0.00  | 1.4                     | -               |
| AORSA-CQL3D   | 74.3 | 24.0         | 1.5                     | 0.2             |

TABLE VII: Comparisons of heating partitions (%) for pre-activation bulk He<sup>4</sup> case 4 with  $n_H/n_e=0.2$ . No beams are active in this case.

| Code          | He <sup>3</sup> | electrons   | thermal H | beam H | carbon impurity |
|---------------|-----------------|-------------|-----------|--------|-----------------|
| PTRANSP-aniso | 29.1            | 42.1 / 7.0  | 21.4      | 0.4    | 0.0             |
| AORSA-iso     | 23.0            | 69.4        | 7.5       | N.A.   | 0.03            |
| CYRANO-iso    | 31              | 64          | 5         | N.A.   | <0.1            |
| EVE-aniso     | 17.2            | 68.2        | 13.5      | 1.2    | 0.0             |
| EVE-iso       | 15.6            | 68.9        | 14.5      | 1.0    | 0.0             |
| TORIC-iso     | 9.7             | 66.3 / 11.3 | 12.1      | 1.0    | 0.0             |
| AORSA-CQL3D   | 12.4            | 78.4        | 9.0       | N.A.   | 0.03            |

TABLE VIII: Comparisons of heating partitions (%) for pre-activation bulk H case 2 with  $n_{He^3}/n_e=0.03$ . The PTRANSP-aniso and TORIC-iso partitions to electrons are split to fast wave and IBW.

| Code          | He <sup>3</sup> | electrons  | thermal H | beam H | carbon impurity |
|---------------|-----------------|------------|-----------|--------|-----------------|
| PTRANSP-aniso | 76.3            | 17.1 / 1.4 | 4.5       | 0.7    | 0.0             |
| AORSA-iso     | 79.1            | 18.8       | 2.1       | N.A.   | 0.1             |
| CYRANO-iso    | 51              | 45         | 4         | N.A.   | <0.1            |
| EVE-aniso     | 45.2            | 37.7       | 9.2       | 7.9    | 0.0             |
| EVE-iso       | 58.1            | 30.0       | 5.6       | 6.3    | 0.0             |
| TORIC-iso     | 53.6            | 36.7 / 1.1 | 7.7       | 0.85   | 0.0             |
| AORSA-CQL3D   | 64.0            | 30.0       | 5.9       | N.A.   | 0.09            |

TABLE IX: Comparisons of heating partitions (%) for pre-activation bulk H case 3 with  $n_{He^3}/n_e=0.2$ . The PTRANSP partition to electrons is further split to fast wave and IBW when available.

| Full-wave solver | He <sup>3</sup> / n <sub>e</sub> | tritium | deuterium | minority | ash | electrons | argon | beryllium | D-beams | alphas |
|------------------|----------------------------------|---------|-----------|----------|-----|-----------|-------|-----------|---------|--------|
| AORSA-CQL3D      | 2%                               | 15      | 0.9       | 50       | 0.3 | 33        | 0.2   | 0.3       | 0       | 0      |
|                  | 0.2%                             | 51      | 2         | 9        | 0.1 | 36        | 0     | 0         | 0.5     | 1.7    |
| CYRANO           | 3%                               | 14      | 0         | 46       | NA  | 39        | NA    | NA        | NA      | 1      |
|                  | 2%                               | 18      | 1         | 41       | NA  | 39        | NA    | NA        | NA      | 1      |
|                  | 1%                               | 25      | 1         | 27       | NA  | 46        | NA    | NA        | NA      | 1      |
|                  | 0%                               | 38      | 1         | 0        | NA  | 60        | NA    | NA        | NA      | 1      |
| EVE-aniso        | 2%                               | 12.9    | 0.4       | 52.8     | 0.1 | 39.1      | 1.4   | 0.2       | 0.0     | 0.2    |
| EVE-iso          | 2%                               | 13.5    | 0.5       | 51.7     | 0.1 | 32.2      | 1.6   | 0.3       | 0.0     | 0.2    |
| EVE-aniso        | 1%                               | 44.2    | 3.1       | 14.1     | 0.2 | 37.9      | 0.0   | 0.0       | 0.2     | 0.4    |
| EVE-iso          | 1%                               | 44.8    | 3.2       | 12.9     | 0.2 | 38.5      | 0.0   | 0.0       | 0.1     | 0.4    |

TABLE X: Comparisons of heating partitions (%) for the DT case 1 as the He<sup>3</sup> fractions are reduced. For the EVE results, due to the presence of the Alfvén Resonance Wave layer on the high field side which results in spurious damping of the wave by the Argon, the power split is estimated at normalized radius = 0.9.

| Poloidal modes | radial points | 1 <sup>st</sup> harmonic T | fundamental He <sup>3</sup> | el fast wave | el IBW |
|----------------|---------------|----------------------------|-----------------------------|--------------|--------|
| 31             | 203           | 12.44                      | 58.65                       | 27.41        | 0.20   |
| 31             | 403           | 12.36                      | 58.71                       | 27.20        | 0.20   |
| 63             | 403           | 13.12                      | 61.18                       | 24.50        | 0.16   |
| 127            | 403           | 13.26                      | 61.00                       | 24.48        | 0.25   |
| 127            | 803           | 13.23                      | 61.10                       | 24.42        | 0.24   |
| 255            | 803           | 13.04                      | 61.12                       | 24.71        | 0.27   |

TABLE XI: *TORIC* results for heating partitions (%) for the DT case 1, but at an earlier time (149s). Convergence study.

| Case | effective T <sub>min</sub> | bulk ion species | electrons | carbon | minority species | beam species |
|------|----------------------------|------------------|-----------|--------|------------------|--------------|
| 2    | anisotropic                | 14.1             | 56.3      | 0.0    | 28.5             | 1.1          |
|      | isotropic                  | 14.7             | 61.8      | 0.0    | 22.7             | 0.8          |
| 3    | anisotropic                | 8.4              | 31.4      | 0.0    | 56.9             | 3.3          |
|      | isotropic                  | 5.5              | 24.7      | 0.0    | 67.7             | 2.1          |
| 4    | anisotropic                | 1.0              | 25.0      | 0.1    | 73.9             | N.A.         |
|      | isotropic                  | 1.0              | 20.1      | 0.1    | 78.2             | N.A.         |

TABLE XII: *EVE* results for heating partitions (%) for the pre-activation cases assuming isotropic or anisotropic effective temperatures. The bulk ion species is H for cases 2 and 3, and He<sup>4</sup> for case 4.

| Equil geometry | tritium | deuterium | minority | ash  | el fast wave | el IBW | alphas |
|----------------|---------|-----------|----------|------|--------------|--------|--------|
| Asymmetrical   | 18.4    | 0.11      | 63.3     | 0.02 | 17.35        | 0.79   | 0.08   |
| Symmetrical    | 18.6    | 0.10      | 67.0     | 0.02 | 13.59        | 0.64   | 0.08   |

TABLE XIII: *PSTELION* results for heating partitions (%) for the DT case 1 assuming either asymmetric or symmetric equilibria.

| He <sup>3</sup> effective temp | hydrogen | minority | electrons | H-beams |
|--------------------------------|----------|----------|-----------|---------|
| 10 [keV]                       | 20.5     | 6        | 73        | 0.5     |
| 14 [keV]                       | 19       | 36       | 49        | ≪ 1     |

TABLE XIV: *TORIC* results for heating partitions (%) for the pre-activation bulk H cases with two assumptions about the minority energy.

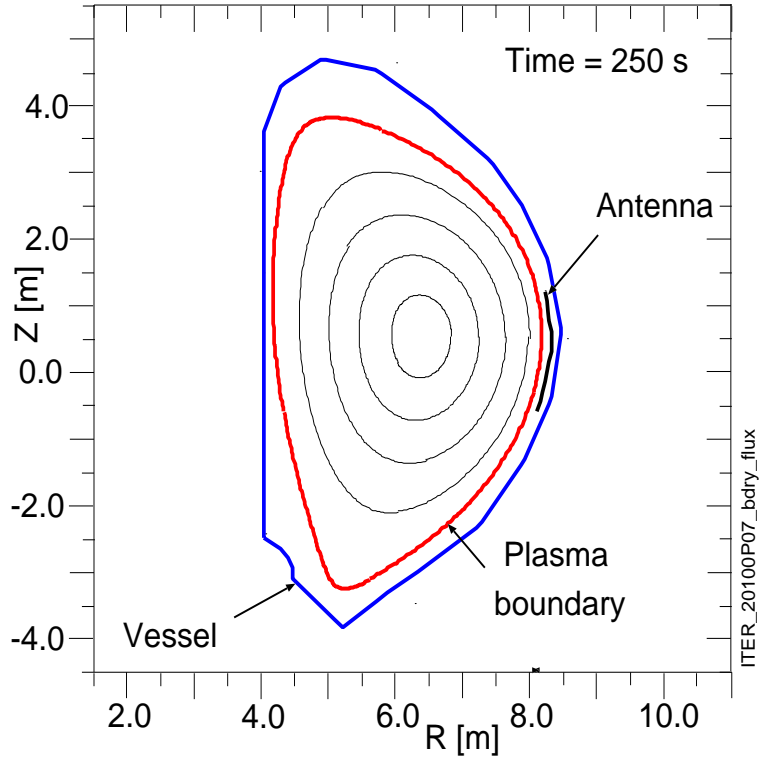


FIG. 1: Assumed boundary and computed flux surfaces for the DT case 1.

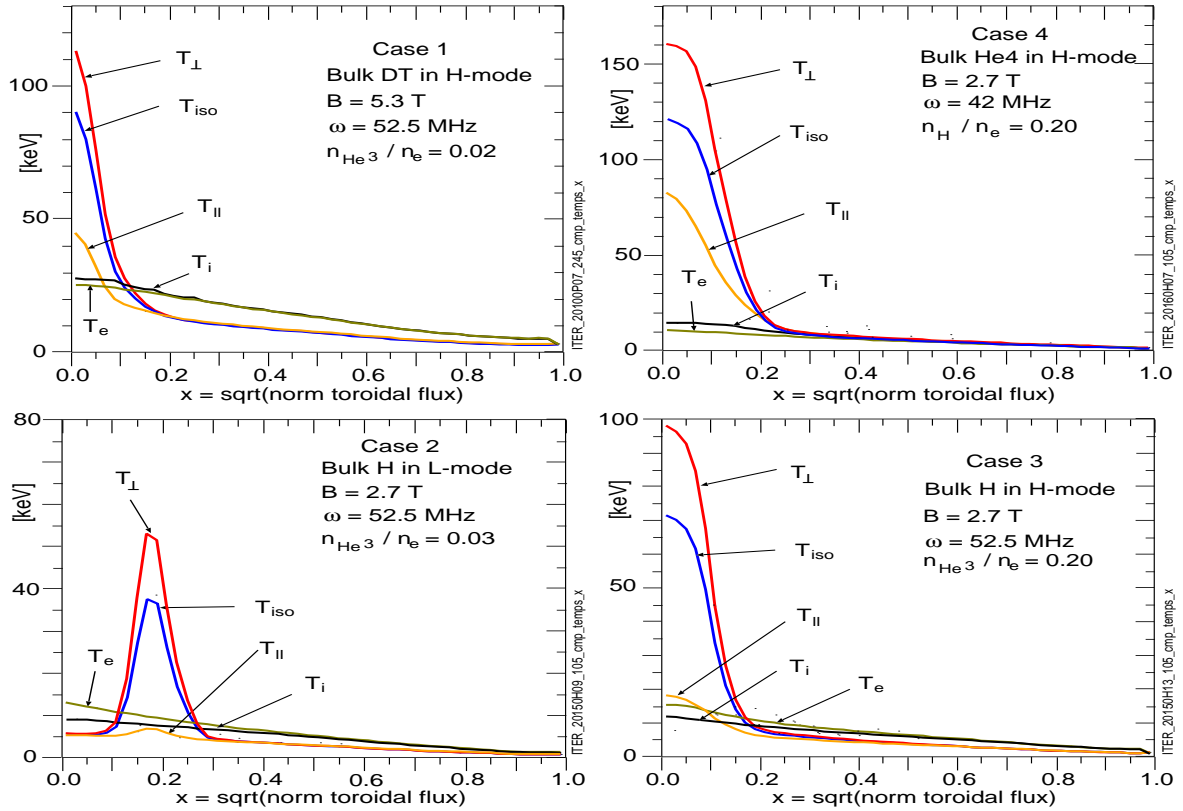


FIG. 2: Temperature profiles for the benchmark cases, computed from PTRANSF using GLF23 for the plasma and FFPRF for the minority ions using Eq. 2.

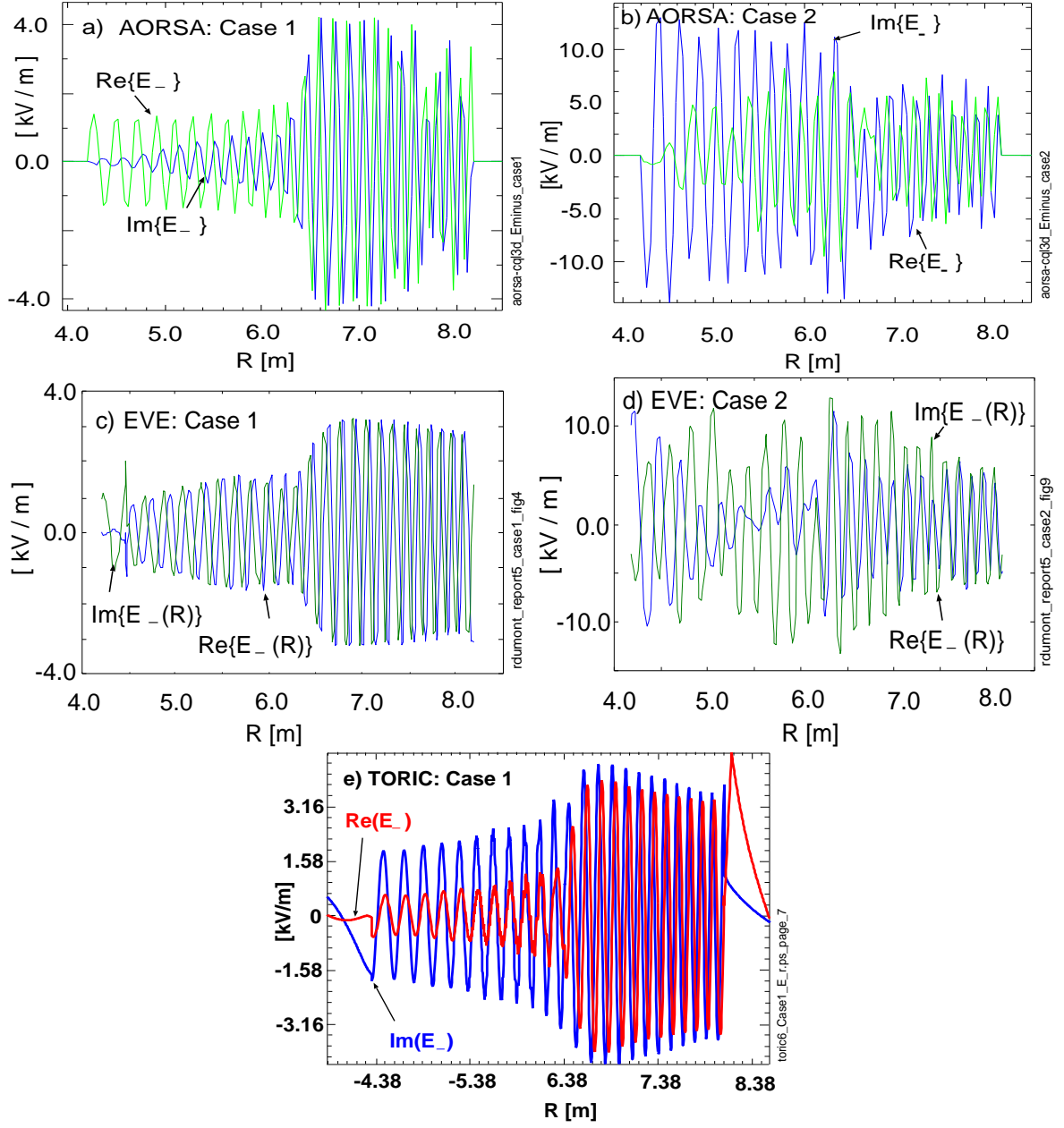


FIG. 3: Profiles along the midplane at the height of the magnetic axis for cases 1 (with fundamental resonance  $\text{He}^3$ ) and 2 (with second harmonic  $\text{He}^3$ ) from a-b) AORSA-CQL3D simulations of  $E_\alpha$  (where the  $\alpha$  unit vector is that part of the  $x$  unit vector that is perpendicular to  $B$ ), c-d) EVE simulations of  $E_-$ , and e) TORIC (v6) simulations of  $E_-$ . The magnetic axis is near 6.38 m

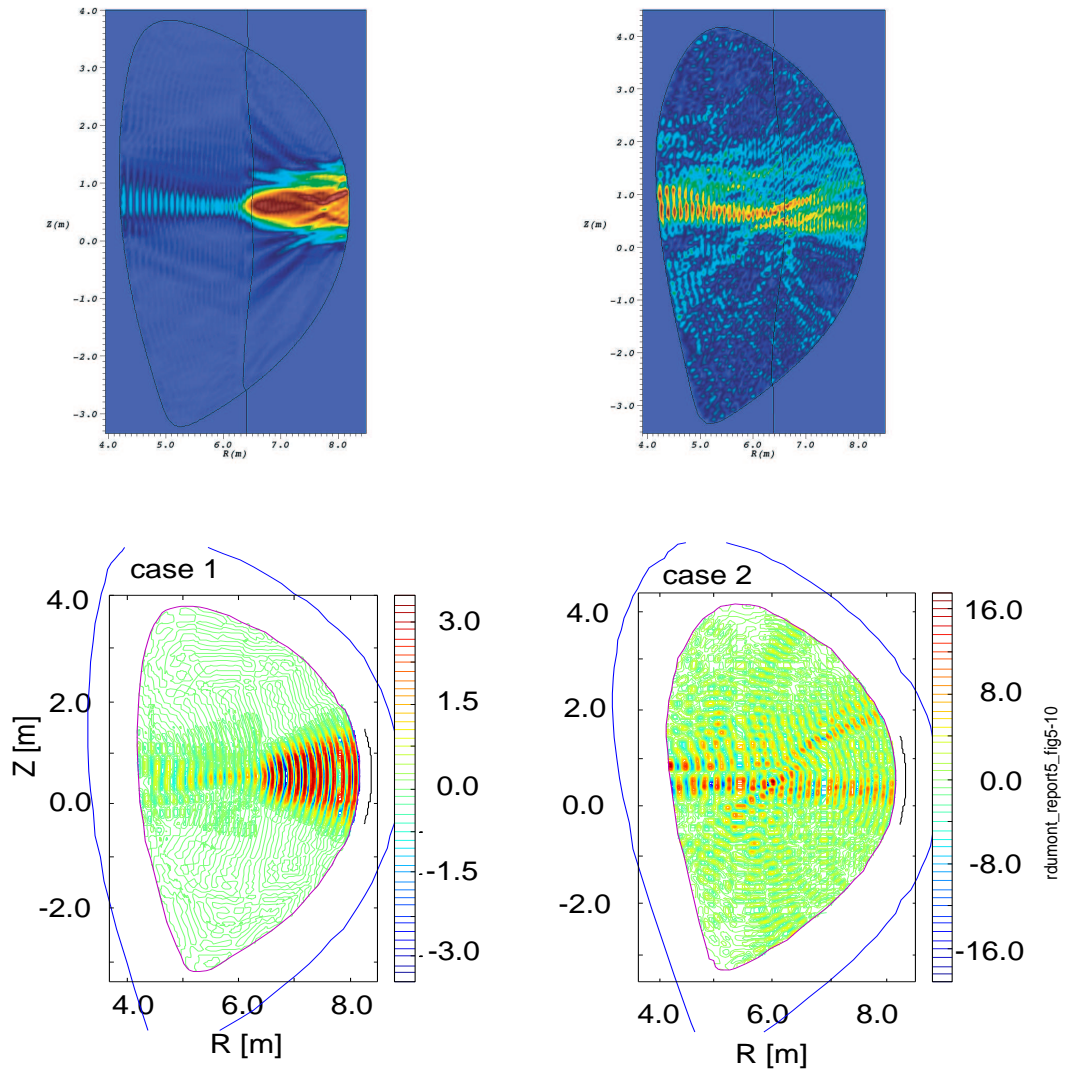


FIG. 4: Contours of the real part of components of  $\text{Re}[E_-]$  for cases 1 and 2 simulated by a) AORSA case 1; b) AORSA Case 2; c) EVE-iso for case 1; d) EVE-iso for case 2. Single-pass absorption is stronger for case 1.

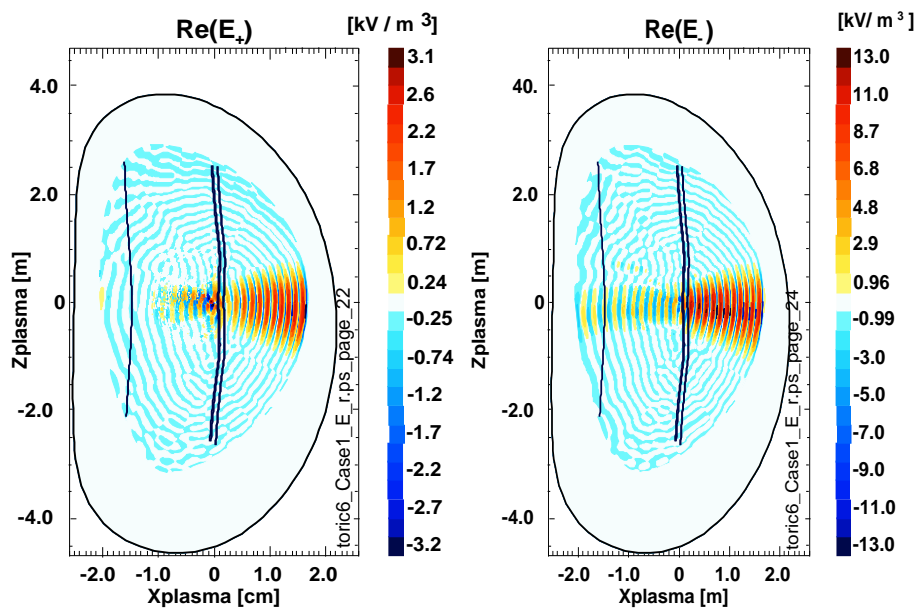


FIG. 5: TORIC simulations of contours of  $\text{Re}[E_+]$  and  $\text{Re}[E_-]$  for case 1, in units of  $[\text{kV}/\text{m}^3]$ . The major radius and vertical displacements are measured relative to the magnetic axis shown in [figure 1](#).

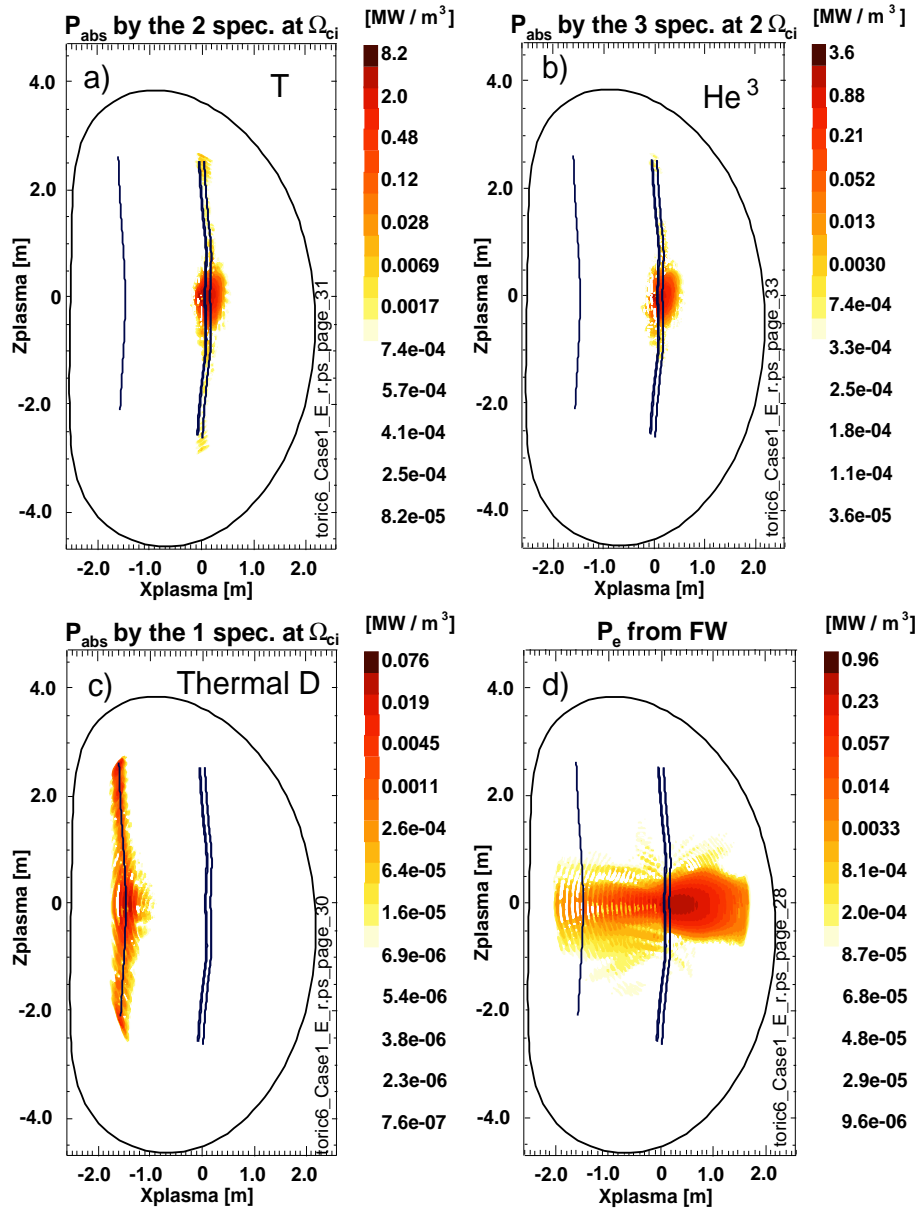


FIG. 6: TORIC simulations of contours of power deposited for case 1 in units of  $[MW/m^3]$ .

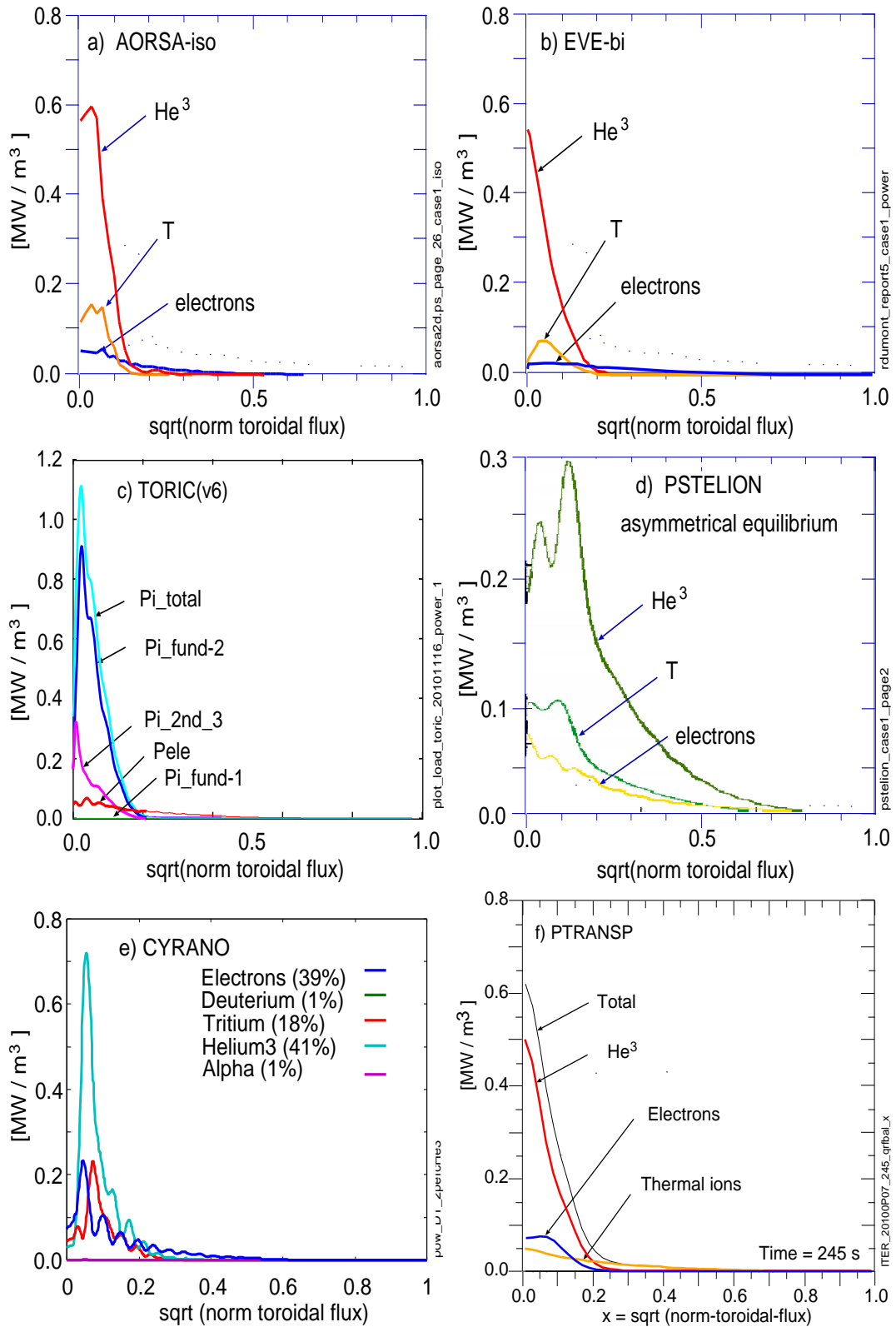


FIG. 7: Simulations of the direct RF-plasma heating power density profiles for the DT case 1 (with 2% He<sup>3</sup>).

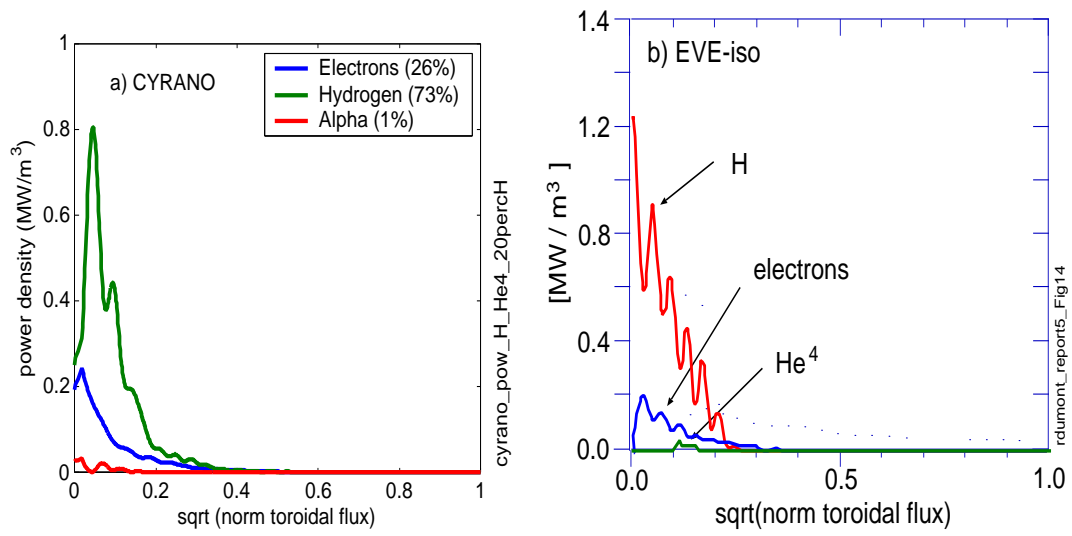


FIG. 8: Simulations of the direct RF-plasma heating power density profiles for the bulk He<sup>4</sup> case 4 (with 20% H) from a) CYRANO, and b) EVE.

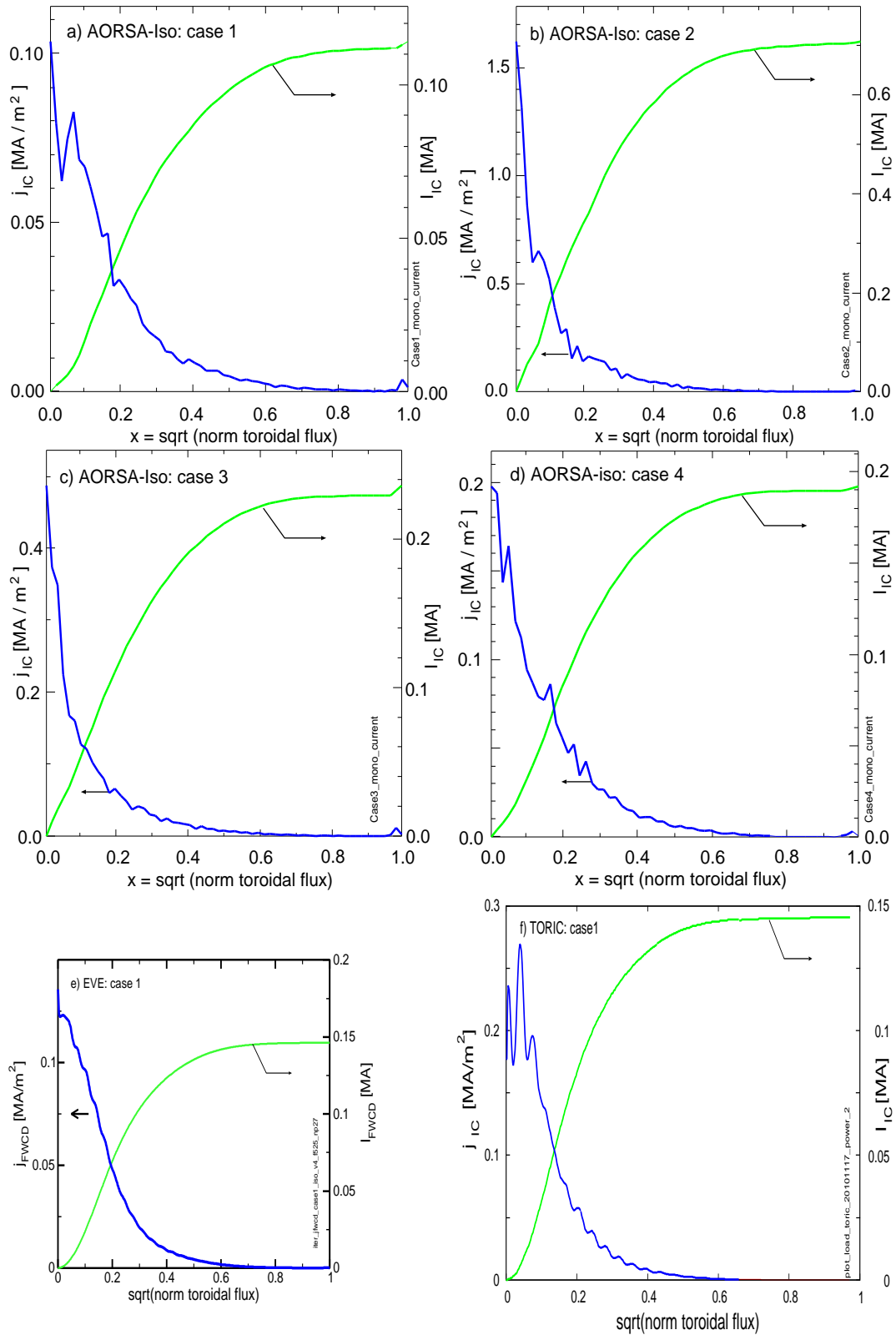


FIG. 9: AORSA-Iso, EVE, and TORIC-v6 simulations of ICRF-driven current profiles and their area-integrals.

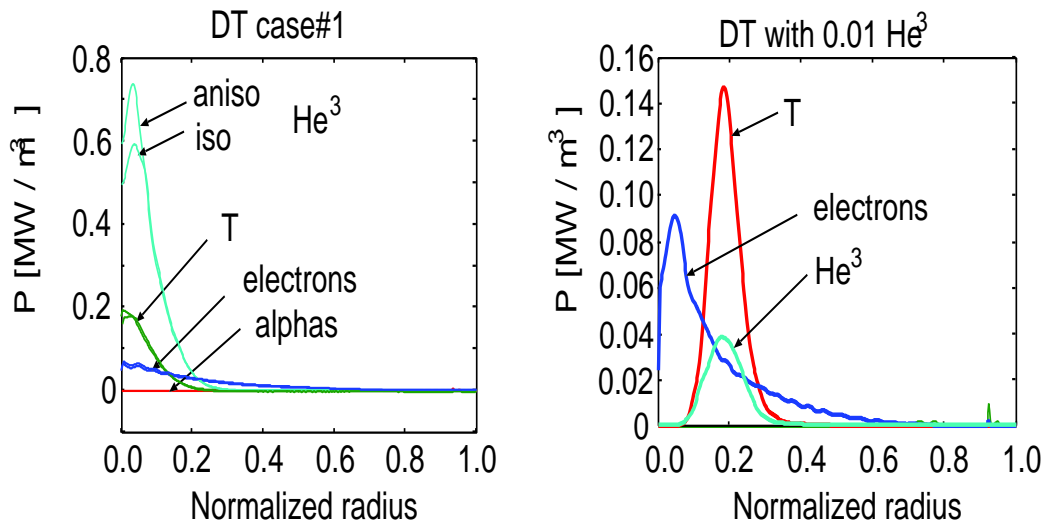


FIG. 10: Simulations of heating power profiles for the DT cases 1 from EVE. a) comparison of isotropic and anisotropic temperatures; b) comparison of  $n_{he3}/n_e = 0.02$  and  $0.001$ , using anisotropic temperatures. The tritium heating increases from 15 to 51%.

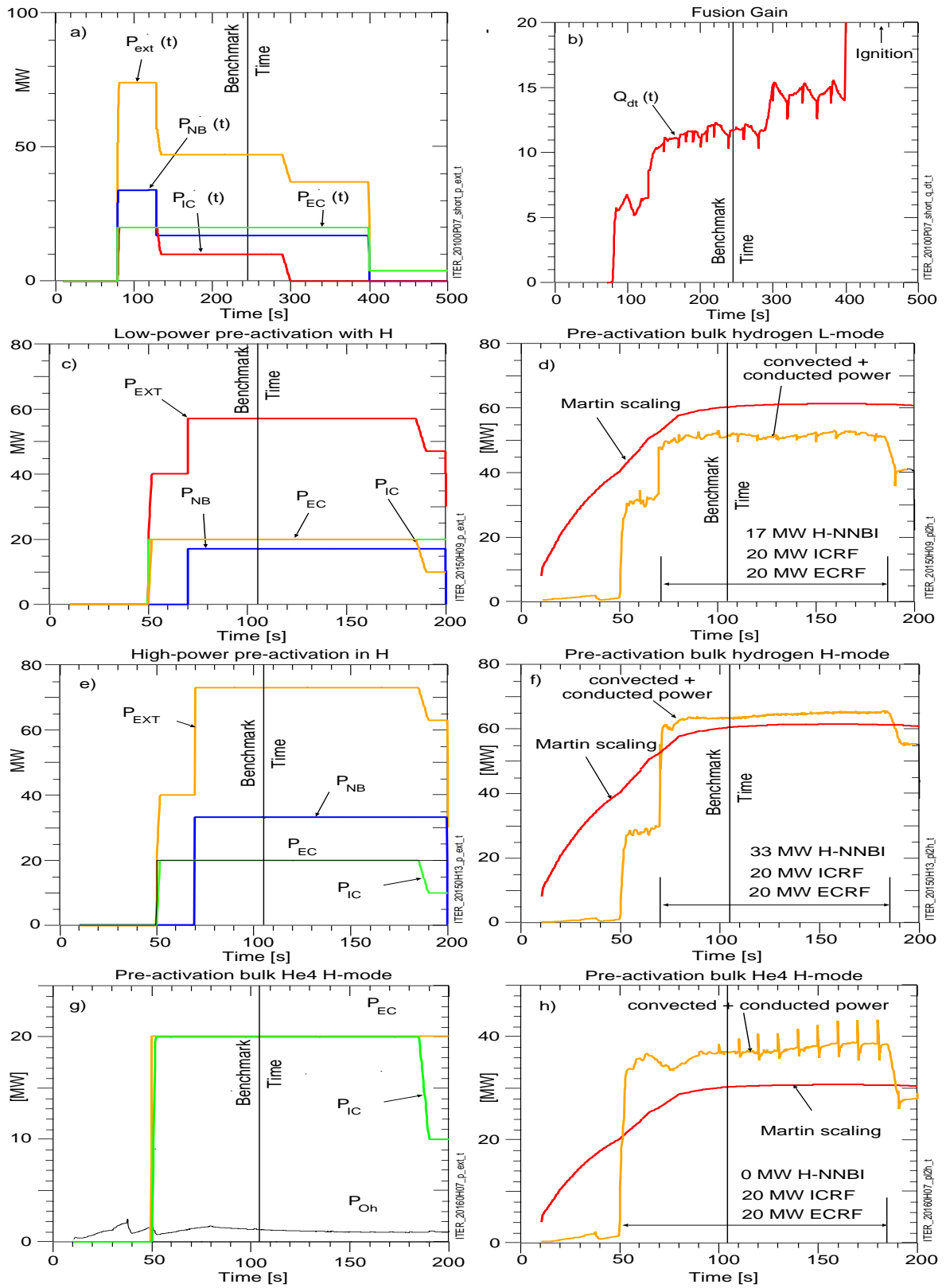


FIG. 11: Waveforms from PTRANSP predictions.

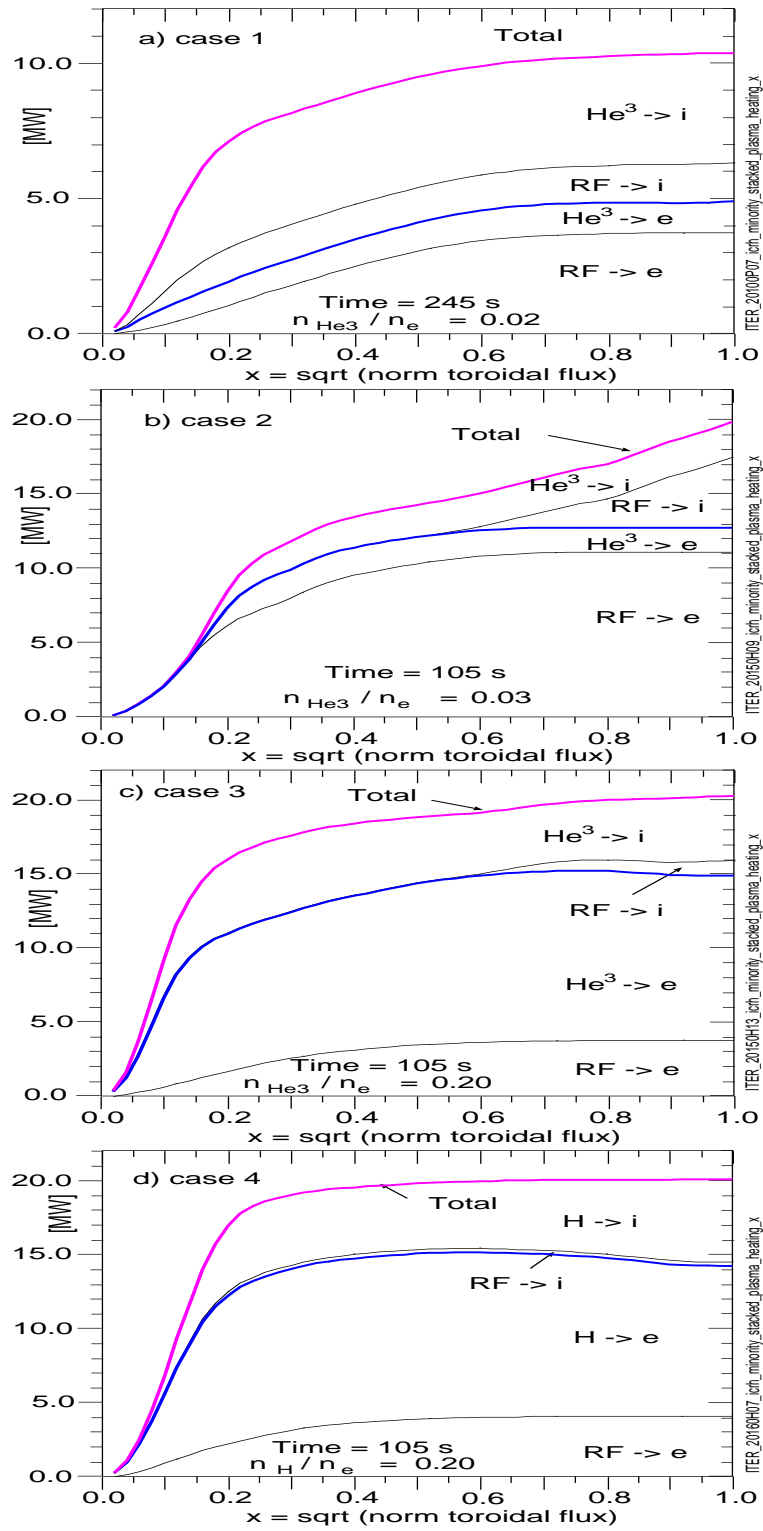


FIG. 12: Stacked ICRF and minority heating profiles for the benchmark cases, computed from PTRANSF-FPPRF.

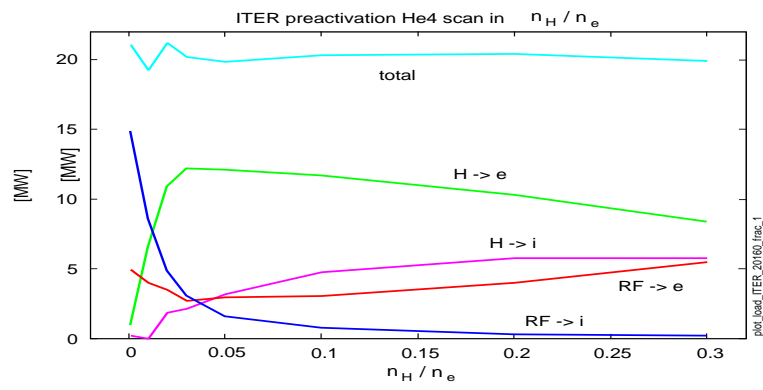


FIG. 13: Total ICRF and minority heating powers for the pre-activation  $\text{He}^4$  case as the fraction of the H-minority is varied. The summed ICRF and minority heating of thermal ions and electrons is needed for transport modeling.



The Princeton Plasma Physics Laboratory is operated  
by Princeton University under contract  
with the U.S. Department of Energy.

Information Services  
Princeton Plasma Physics Laboratory  
P.O. Box 451  
Princeton, NJ 08543

Phone: 609-243-2245  
Fax: 609-243-2751  
e-mail: [pppl\\_info@pppl.gov](mailto:pppl_info@pppl.gov)  
Internet Address: <http://www.pppl.gov>